spectra recorded in the interior of the solution grown ruthenium film when compared to a static SIMS positive ion spectrum recorded from sputtered cleaned metallic Ru as illustrated in Figure 8. The two major features in Figure 8 are the species corresponding to the mass of Ru and RuO. Ruthenium has seven natural isotopes and their natural abundances in percent are as follows: ^{96}Ru, 5.5; ^{98}Ru, 1.9; ^{99}Ru, 12.7; ^{100}Ru, 12.6; ^{101}Ru, 17.1; ^{102}Ru, 31.6; ^{104}Ru, 18.6. The observed ion intensity distribution shown in Figure 8 for both Ru ions and RuO ions matches perfectly with the ruthenium natural abundance pattern. The ruthenium in the metallic thin film appears to be much purer than commercially available ruthenium metal as is indicated in Figure 7 by the fact that the SIMS spectrum of the Ru thin film lacks a feature at m = 137 which was assigned to barium. The observation of suboxide RuO fragments indicates the presence of Ru–O bonds in the Ru mirror films. Masses corresponding to ruthenium dioxide and trioxide were not found in these metallic mirror thin films.

Conclusions

Smooth, shiny, metallic Ru mirrors were successfully fabricated via a TMPEDTA adhesion layer between the interface of Ru and fused quartz. The chemical composition of these Ru mirrors was analyzed by AEP, XPS, SIMS, and RBS, and these surface characterizations indicate that the thin metallic film consists of mainly Ru metal. Infrared spectroscopy reveals that the Ru mirrors reflect infrared radiation perfectly; therefore, application of these low-cost Ru mirrors in infrared instruments is plausible. The smoothness suggested by STM and SEM is far below the order of micrometers, which implies that the Ru mirrors are extremely smooth to light waves in the infrared region.

Registry No. TMPEDTA, 84127-79-7; $Ru(H_2O)_6^{2+}$, 30251-71-9; SiO_2, 60676-86-0; Ru, 7440-18-8; Si, 7440-21-3.

Mixed-Metal Amorphous and Spinel Phase Oxidation Catalysts: Characterization by X-ray Diffraction, X-ray Absorption, Electron Microscopy, and Catalytic Studies of Systems Containing Copper, Cobalt, and Manganese

Paul A. Wright,* Srinivasan Natarajan, and John M. Thomas*

The Davy Faraday Research Laboratory, The Royal Institution of Great Britain, 21 Albemarle Street, London W1X 4BS, UK

Pratibha L. Gai-Boyes

Central Research & Development, E. I. Du Pont de Nemours, Experimental Station, Wilmington, Delaware 19880-0356

Received April 1, 1992. Revised Manuscript Received June 8, 1992

Mixed-metal carbonates $CuMn_2(CO_3)_3$, $CuMn(CO_3)_2$, $CoMn_2(CO_3)_3$, and $CuCoMn(CO_3)_3$ possessing the rhodocrosite structure have been prepared by coprecipitation. Extended X-ray absorption fine structure (EXAFS) analysis indicates that cobalt substitutes fully and without distortion into the rhodocrosite structure in $CoMn_2(CO_3)_3$, whereas copper is present in $CuMn_2(CO_3)_3$ in a distorted environment. Decomposition at temperatures of ca. 600 K for $CuCoMn(CO_3)_3$ and ca. 690 K for the other carbonates yields amorphous or (for the $CoMn_2$ system) very poorly crystalline oxides. EXAFS analyses of these solids reveals that cobalt and manganese ions order to the second and higher coordination shells in proto-spinel structures faster than do ions of copper. The majority of manganese and cobalt cations have 6-fold and most copper 4-fold coordination in the just-decomposed oxides, although in the poorly crystalline $CoMn_2$ oxide around one-third of the cobalt ions are in tetrahedral sites. Heating the carbonates to 773 K in air produces spinels that are phase pure by X-ray diffraction: whereas the copper-bearing spinels are cubic, $CoMn_2O_4$ is tetragonal. Copper occupies mainly tetrahedral sites in these spinels, although the presence of some octahedral copper is clearly revealed by EXAFS. This increases in the order $CuCoMnO_4 < CuMn_2O_4 < Cu_{1.5}Mn_{1.5}O_4$. Manganese is predominantly octahedral in all of the spinels (Jahn–Teller distortion in $CoMn_2O_4$) and cobalt is octahedral in $CuCoMnO_4$ and occupies both sites in $CoMn_2O_4$, ordering on to the tetrahedral site upon heating. On the basis of EXAFS and X-ray absorption near-edge spectral (XANES) analyses and assuming the spinels are stoichiometric, we infer that copper is present in the spinels as a mixture of 1+ and 2+ ions. In $CuMn_2O_4$ and $CuCoMnO_4$ the manganese is present as a mixture of 3+ and 4+ and in $CoMn_2O_4$ predominantly as 3+. Cobalt is 3+ in $CuCoMnO_4$ and a mixture of 2+ and 3+ in $CoMn_2O_4$. Many of the oxides catalyze the complete reaction of an undiluted 2:1 CO/O_2 gas mixture at room temperature, so that dilution of both the gas mixture and the catalyst itself was performed to give conversions less than 100% between 60 and 160 °C. Amorphous oxides in the Cu/Mn and Co/Mn systems have slightly higher specific activities than the corresponding spinels. Of all the mixed-metal oxides prepared, the $CuCoMnO_4$ spinel has both the highest specific activity, probably due to the cobalt being largely trivalent, as well as the highest surface area.

Introduction

The ability of amorphous manganese oxides promoted by transition metals to catalyze the oxidation of carbon monoxide and hydrocarbons, even at ambient temperature, has long been known.[1] Amorphous manganese oxide with added copper, known as hopcalite, has been studied to

(1) Jones, H. A.; Taylor, H. S. *J. Phys. Chem.* **1923**, *27*, 623.

0897-4756/92/2804-1053$03.00/0

clarify the importance of the effects of the copper–manganese redox couple,[2] the copper oxidation state and coordination,[3] the crystalline structure and surface area, and the presence of surface inhibitors.[4] Spinels of similar composition are also active, and surface measurements on multiphase mixed oxides of cobalt, copper, and manganese prepared by heating coprecipitated hydroxides suggest that their catalytic activity can be rationalized in terms of the abundance at the surface of the more active copper and cobalt ions in their higher oxidation states.[5]

We have adapted preparation conditions given in the literature[6-8] for the synthesis of manganese-rich carbonates of the rhodocrosite ($MnCO_3$, calcite-like) structure, which include copper and cobalt in solid solution. Coprecipitation on an intimate scale followed by thermal decomposition allows the preparation of mixed oxides at lower temperatures (because diffusion distances are reduced) compared to traditional solid-state procedures. In particular, if two metals crystallize in a solid solution within the same structure, mixing on an atomic scale is achieved. At least some solid solution, as indicated by reduction of unit cell parameters of the rhodocrosite structure upon substitution of smaller Co^{2+} and Cu^{2+} cations for Mn^{2+}, has been demonstrated for the Cu/Mn[8] and Co/Mn[7] systems. Using our modified procedure we have quantitatively precipitated Cu and Mn, Co and Mn, and Cu, Co, and Mn and determined the extent to which the nonmanganese cation(s) substitute into the rhodocrosite structure using a combination of X-ray diffraction, electron microscopy, X-ray absorption, and thermogravimetric analysis.

In addition to producing oxides of relatively high surface area, the low temperatures of decomposition of these mixed carbonates[9] enable metastable cation configurations or crystal structures to be produced as intermediates. Indeed, the coordination of surface copper in hopcalite was inferred from X-ray photoelectron spectroscopy (XPS) data to change from octahedral 2+ to tetrahedral 1+ upon crystallization into the spinel structure.[3,4] The precursor carbonates were therefore decomposed in air under conditions that formed (a) amorphous or poorly crystalline oxides and (b) spinels, single phase to X-ray diffraction. The poor crystallinity of the "just-decomposed" oxides and the deliberately chosen similarity of atomic number of the metal cations prevent the determination of site occupancies by X-ray diffraction. We consequently made use of the element specificity of X-ray absorption by performing measurements at the Cu, Co, and Mn K-edge to enable details of the cation distribution in both the crystalline and the amorphous solids to be resolved. Electron microscopy was used to determine the textural and microstructural details and check the homogeneity and phase purity of the samples.

The catalytic activity of these oxides for the low-temperature oxidation of carbon monoxide was measured and rationalized in terms of crystallinity and surface area and, bearing in mind the likely differences between bulk and surface compositions,[5] comparisons were made between spinels of different cation content.

Experimental Section

The samples were prepared according to the method for calcium-bearing carbonates in the calcite structure,[7] with temperatures modified according to ref 8. A 0.5 M solution of a mixture of the metal nitrates (in the desired stoichiometry) was added dropwise and with constant stirring to an excess of a heated 0.5 M solution of sodium bicarbonate through which carbon dioxide was continuously bubbled. The resulting precipitate was filtered and thoroughly washed with cool distilled water, with analyses showing very low levels of sodium remained. The samples were dried in air at 60 °C, and their crystallinity was checked by X-ray diffraction. The carbonates were analyzed for cations and sodium by inductively coupled plasma (ICP) emission spectroscopy to check that precipitation was quantitative. While pure manganese nitrate and the mixed nitrates give carbonates of the rhodocrosite structure, the addition of pure copper nitrate yields a malachite phase and of cobalt nitrate yields an amorphous precipitate.

Thermogravimetric analysis was performed on a Stanton-Redcroft thermal analyzer (model No. STA 1000/1500). The temperature was increased at 10 °C/min to 600 °C under a constant flow (45–50 mL/min) of air.

The thermal decomposition of the carbonates in air was followed using in situ X-ray diffractometry (rotating anode X-ray source operating at 8 kW, copper target, Siemens D500 diffractometer) to examine the course of the reaction. On the basis of these results, the carbonates were heated for 1 h in air in a muffle furnace under conditions (a) suitable to just decompose the carbonate and resulting in a minimum of X-ray crystallinity and (b) at a temperature (500 °C) at which the products were single-phase spinels (by X-ray diffraction). For the $CoMn_2$–carbonate, intermediate temperatures were used to follow the transition from a cubic to a tetragonal phase. Thermal decomposition of the pure metal carbonates and hydroxycarbonates at 500 °C gave CuO, Co_3O_4 and for manganese, a mixture of Mn_2O_3 (JCPDS No. 31-825) and $Na_{0.2}MnO_2$ (JCPDS No. 27-747). Full details of preparation and TGA and XRD characterization of carbonates and oxides are given in Table I. The oxide samples are identified by the metal stoichiometry and the temperature at which they had been heated.

Electron microscopic analysis was carried out on a CM30 ST 300-kV instrument fitted with a STEM unit and with a completely windowless EDX detector for simultaneous microanalysis. (The super-twin lens configuration has a coefficient of spherical aberration, Cs, of 1 mm at 300 kV, with a resolution of <2 Å for high-resolution imaging (HREM) and a couple of nanometers for microanalysis; convergent beam diffraction; and high magnification up to 10^6). Samples for HREM were microtomed to preserve particle morphology. Additional SEM analysis was performed on a Cambridge stereoscan 200 fitted with an EDX detector for bulk analysis.

Room-temperature X-ray absorption measurements were carried out over the Cu, Co, and Mn K-edges on station 7.1 at the SERC Daresbury synchrotron X-ray source, using a Si(111) double-crystal monochromator. Spectra on model compounds of known crystal structure (CuO, Cu_2O, CoO, Co_3O_4, MnO, Mn_2O_3, and MnO_2) were collected to determine and check the transferability of the atom-specific parameters necessary for fitting data on the mixed metal oxides. Data were collected out to around 15 $Å^{-1}$, with collection times typically around 40 min. X-ray spectra were analyzed using the suite of programs available at Daresbury, including the normalization and background subtraction program EXBROOK and the curve-fitting and refinement program EXCURV90. The EXAFS function was obtained from EXBROOK and transferred to EXCURV90 for fitting. Within EXCURV90 the EXAFS of model compounds of known structure were fitted by allowing atom-specific parameters to refine within reasonable values. The atom-specific parameters for copper–oxygen and copper–copper interactions were fitted for CuO and found to fit Cu_2O very well. The parameters for manganese–oxygen and

(2) Schwab, G.-M.; Kanungo, S. B. *Z. Phys. Chem. (Munich)* **1977**, *107*, 109.
(3) Yoon, C.; Cocke, D. L. *J. Catal.* **1988**, *113*, 267.
(4) Veprek, S.; Cocke, D. L.; Kehl, S.; Oswald, H. R. *J. Catal.* **1986**, *100*, 250.
(5) Yang, B. L.; Chan, S. F.; Chang, W. S.; Chen, Y. Z. *J. Catal.* **1991**, *130*, 52–61.
(6) Longo, J. M.; Horowitz, H. S.; Clavenna, L. R. In *Solid State Chemistry: A Contemporary Overview*; Advances in Chemistry Series, 186; Holt, S. L., Milstein, J. D., Robbins, M., Eds.; American Chemical Society: Washington, DC, 1980; No. 139.
(7) Vidyasagar, K.; Gopalakrishnan, J.; Rao, C. N. R. *Inorg. Chem.* **1984**, *23*, 1206.
(8) Porta, P.; Moretti, G.; Lo Jacono, M.; Musicanti, M.; Nardella, A. *J. Mater. Chem.* **1991**, *1*, 129.
(9) Porta, P.; Moretti, G.; Musicanti, M.; Nardella, A. *Catal. Today* **1991**, *9*, 211.

Table I. Details of Preparation and Composition and Carbonate and Spinel Cell Dimensions[a]

sample (stoichiometry)	ppttn temp, °C	color	composition, mol % metals				carbonate[b] unit-cell param, Å		TGA wt loss			spinel[c] unit cell param, Å	
			Cu	Co	Mn	Na	a	c	10% °C	90% °C	total, wt %	a	(c)
Mn	80	off-white					4.776 (5)	15.695 (22)	400	470	27.8	5.765[d]	9.442[d]
Co	60	pink					4.662[d]	14.963[d]	80	300	29.8	8.084 (3)	
CuMn2	60	green/yellow	32.3	0.0	67.7	<0.5 ppm	4.741 (3)	15.485 (11)	345	395	35.5	8.297 (5)	
CuMn	60	green	48.4	0.0	51.6	ND	4.726 (11)	15.46 (20)	170	425	26.1	8.296 (6)	
CoMn2	60	purple	0.0	32.5	67.4	<0.5 ppm	4.765 (2)	15.531 (16)	385	415	36.5	5.73 (3)	9.30 (4)
CuCoMn	80	green/grey	33.0	32.6	34.4	ND	4.714 (12)	15.01 (20)	140	400	37.1	8.17 (2)	

[a] Values in parentheses are the estimated errors in the lattice parameters. [b] The carbonate (symmetry R3̄c) is indexed on a hexagonal cell. [c] Spinels are cubic or tetragonal. [d] Literature values; these samples were not prepared. ND: not detected.

manganese–manganese were fitted taking MnO_2 (pyrolusite[10]) as a model compound and checked against MnO (rock salt structure). They gave reasonable agreement, although the distances in MnO were predicted to be about 0.02 Å too low. This should be borne in mind when considering the values given in Table III. Cobalt phase parameters were obtained from CoO (rock salt structure) and gave reasonable agreement with the Co_3O_4 spinel. Using these derived parametes, local cation environments were examined in terms of coordination number, metal-to-oxygen distance, and the Debye–Waller factor. The option within EXCURV90 that performs Fourier filtering of data from particular coordination shells, or groups of coordination shells, was used to examine the EXAFS data. To reduce termination errors in the Fourier filtering, the k_{min} and k_{max} were taken at nodes in the EXAFS function at around 3 and 13–15 $Å^{-1}$, respectively. Models of cation coordination environments were refined by fitting the filtered k^3-weighted EXAFS function. For the best fits the filtered experimental and the fitted theoretical k^3-weighted EXAFS function were plotted, along with the unfiltered experimental and filtered theoretical phase-corrected Fourier transforms. The errors associated with refined parameters[11] are around 10% in the coordination number and Debye–Waller factor and 0.02 Å in the coordination distances.

Preliminary studies of the catalytic performance using a gas mixture of CO and O_2 in the ratio 2:1 over activated amorphous $CuMn_2$-420 at room temperature in a fixed-bed reactor resulted in an exothermic reaction and 100% conversion. To permit comparison between the samples, both the gas mix and the catalyst itself were diluted. In a typical experiment the oxide sample was mixed thoroughly (without grinding) with amorphous quartz in the ratio 1:4; 100 mg of this mixture was used for our tests. The catalyst was activated in moisture-free oxygen at 225 °C for 1 h and slowly cooled to 160 °C, at which temperature the reaction mixture (20 mL/min of 3% CO in helium and 40 mL/min of dry air) was passed over the solid under test. The temperature was dropped stepwise and the degree of conversion monitored at each temperature until the percentage CO conversion was invariant. Pre- and post-reactor gas compositions were analyzed using a gas chromatograph fitted with a TCD detector. As well as the mixed metal oxides, CuO, Co_3O_4, and MnO_x were examined for comparison. Catalyst surface areas were determined by BET analysis of nitrogen adsorption isotherms measured gravimetrically at liquid nitrogen temperature.

Results

(a) Bulk Analysis and X-ray Diffraction. The analyses performed by ICP on the mixed metal carbonates (Table I) show that the bulk molar ratios are very close to those stoichiometries weighed out in the preparation, and that sodium is effectively removed by washing. The crystallinity of the manganese and $CoMn_2$ carbonates are very good, of the $CuMn_2$ moderate, and of the $Cu_{1.5}Mn_{1.5}$ and CuCoMn carbonates very poor (Figure 1). There is consequently considerable error in determining the unit-cell parameters (and particularly the c axis of the hexagonal cell) for the last two. The unit-cell parameters of all of the manganates containing copper and/or cobalt are smaller than those of the pure synthetic rhodocrosite, indicating that the smaller cobalt and copper 2+ ions ($r_{Co^{2+}}$ = 0.89 Å high spin (HS), $r_{Cu^{2+}}$ = 0.87 Å in 6-fold coordination) substitute at least partly for the larger Mn^{2+} ion ($r_{Mn^{2+}}$ = 0.97 Å HS). The rank of the size decreases is also as expected on the basis of an average M^{2+} ion size:

$$Mn > CoMn_2 > CuMn_2 > CuMn > CuCoMn$$

The degree of substitution is less definite. Comparing $CoMn_2$ carbonate with the $CoCO_3$ and $MnCO_3$ end members indicates the mixed carbonate has values much closer to the manganese end member than straightforward prediction according to Vegard's law would predict. However, deviations from Vegard's law are common among solid solutions. No such comparison can be made for the $CuMn_2$-carbonates as copper carbonate does not exist in the calcite structure, but the unit-cell parameters are smaller for the $CuMn_2$ carbonate than for the $CoMn_2$ carbonate, suggesting that similar amounts of copper and cobalt substitution occur. The cell parameters for $CoMn_2$ carbonate and $CuMn_2$ carbonate are very close to those reported elsewhere for similar preparations and described as being solid solutions.[6,8]

In situ X-ray diffractometry of samples heated in air indicates that upon losing crystallinity the samples pass through an amorphous or very poorly crystalline phase and crystallize in the spinel form. Subsequent furnace heating for 1 h at appropriate temperatures allows just decomposed amorphous or poorly crystalline (325–420 °C) and spinel (500 °C, see Figure 2) oxides to be formed. For the $CuMn_2$

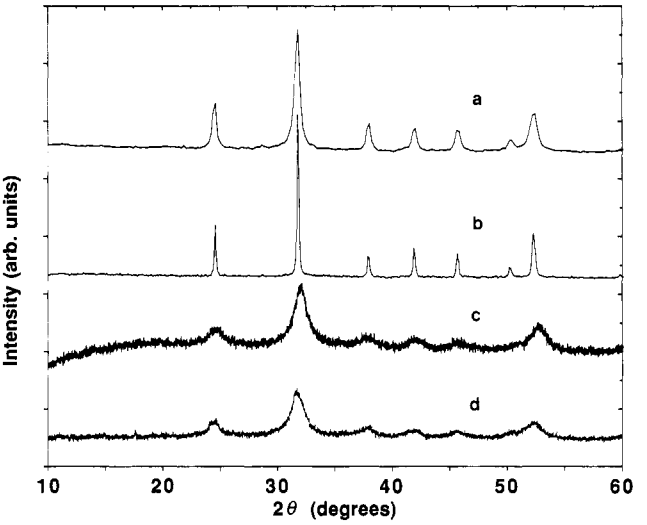

Figure 1. XRD patterns of the precursor carbonates, all crystallized from aqueous solutions (in the rhodocrosite structure) at 60–80 °C: (a) $CuMn_2$, (b) $CoMn_2$, (c) CuCoMn, and (d) $Cu_{1.5}Mn_{1.5}$.

(10) Baur, W. H. *Acta. Crystallogr.* **1976**, *B32*, 2200.
(11) Gurman, S. J. In *Applications of Synchrotron Radiation*; Catlow, C. R. A., Greaves, G. N., Eds.; Blackie: Glasgow, 1990; p 140.

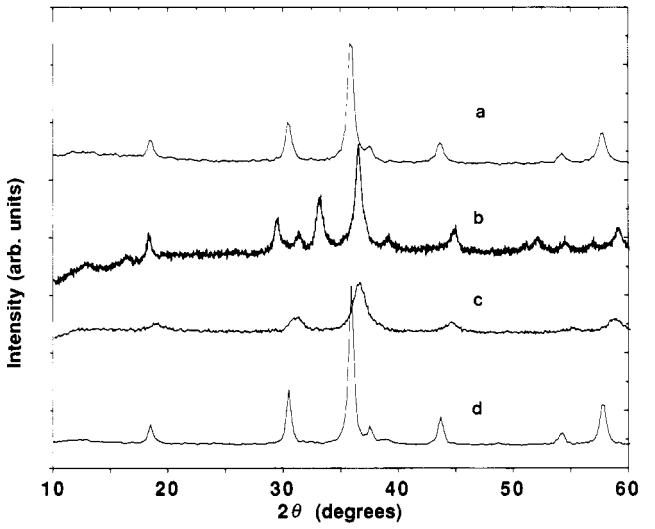

Figure 2. XRD patterns of the spinels formed at 500 °C from the corresponding precursor carbonates shown in Figure 1: (a) $CuMn_2O_4$, (b) $CoMn_2O_4$, (c) $CuCoMnO_4$, and (d) $Cu_{1.5}Mn_{1.5}O_4$. The $CoMn_2O_4$ exhibits a tetragonal distortion: the other three are cubic.

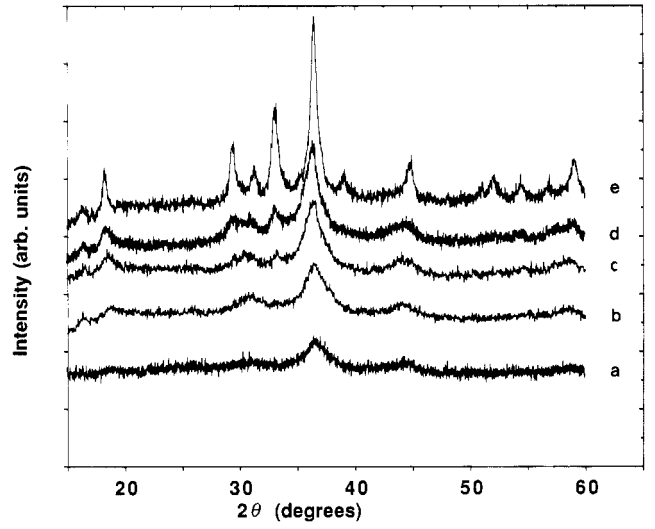

Figure 3. XRD patterns of $CoMn_2O_4$ spinel as a function of decomposition temperature: (a) 415, (b) 430, (c) 450, (d) 475, and (e) 500 °C. On heating, the crystalline $CoMn_2$ carbonate passes through a poorly crystalline cubic phase to the tetragonal phase.

system, a very small carbonate peak remains after heating at 420 °C and an X-ray pure spinel is formed at 500 °C. For the CuMn sample an amorphous phase is formed at 420 °C and a highly crystalline spinel is formed at 500 °C with a trace of copper oxide. For $CoMn_2$, the carbonate decomposes to give a very poorly crystalline cubic spinel, which crystallizes at 500 °C to a tetragonal spinel. This change was monitored at intermediate temperatures (Figure 3). CuCoMn carbonate, itself poorly crystalline, decomposes via an amorphous phase to give a cubic spinel at 500 °C.

(b) Thermogravimetric Studies. Thermogravimetric analyses carried out on the as-prepared carbonates in an atmosphere of flowing air indicate that they start losing water at around 150–200 °C and decomposition starts at around 250–300 °C. The decomposition is complete at about 420 °C for all the precursor carbonates. The temperatures of 10% and 90% weight loss show that the range of $CuMn_2$ and $CoMn_2$ carbonate decomposition is remarkably narrow (30–50 °C), whereas that of $Cu_{1.5}Mn_{1.5}$ and CuCoMn is broader (150–200 °C). This observation confirms that the CuCoMn sample forms an amorphous phase at a much lower temperature compared to other carbonates (325 °C) and may be because of the higher occupancy of non-manganese cations in the rhodocrosite structure, which render it thermally unstable.

(c) Electron Microscopy. Nanometer-scale EDX compositional analysis in the STEM has shown that, in general, the samples exhibit uniform chemical homogeneity throughout the temperature regimes studied. A few grains of the component oxides are occasionally found. The selected area electron diffraction and high-resolution lattice imaging have illustrated the extent of structural order at different temperatures. For example, carbonates of the Cu–Mn and Co–Mn systems and their spinels exhibited very good crystallinity. Samples heated at 500 °C showed most of the microcrystals to be single crystalline with the spinel structure. Some amorphous pockets (ca. 5 nm in dimension) were found in these samples. Samples heated at 325–420 °C contained primarily amorphous regions with a few microcrystals only 5–10 Å in diameter.

Figures 4 and 5 illustrate the microstructural evolution. Figure 4 shows essential characteristics of the $CuMn_2$ stoichiometry, with an SEM image (a) of the carbonate revealing mostly spherical particles which retain their morphology upon heating. A diffraction pattern of the carbonate (b) indicates microcrystallinity: the diffraction rings can be indexed based on the rhodocrosite structure. High-resolution imaging (c) shows microcrystallinity present in the larger spherical spinel particles, with crystallites of the order of 10 nm in size. There is generally no direct evidence of twins or strains at the boundaries where the randomly growing microcrystals happen to meet, suggesting that they relax structurally as they grow. Normally the microcrystals expose planes in the (100), (110), and (111) orientations. The lack of well-defined shapes for the microcrystals may mean that their shape is dictated by the atomic arrangement in the neighboring grains. The selected-area diffraction pattern (d) and the microcompositional analysis (e) are consistent with the spinel structure and the bulk composition. (The Al peak in the EDX spectrum is due to the microscope grid used to support the samples.) Similar results were observed in the CuMn system.

In the $CoMn_2$ system (Figure 5) the carbonate precipitate consists largely of platelike crystals growing in clusters (a–c) which also maintain their morphology upon thermal decomposition. The different shapes in the CuMn and CoMn systems can be attributed to the different surface energetics of the two systems. The individual plates contain microcrystals in different crystallographic orientations. As in the CuMn system the diffraction rings can be indexed on the carbonate structure, although some crystals show longer range crystallinity (d). The $CoMn_2$-430 sample is mainly amorphous, with pockets of crystallinity. The spinel structure formed at 500 °C exhibited microcrystallinity similar to that found in the Cu/Mn system. All samples showed a high degree of chemical uniformity to nanometer scale microanalysis.

In the Cu–Co–Mn system the particles are spheres around 10 μm in diameter. The crystallites are smaller, with a crystallite size around 6 nm estimated both from the electron micrographs (Figure 6a) and Debye–Scherrer broadening of the X-ray pattern. Furthermore, both the carbonates and the 500 °C spinels show poorer crystallinity relative to the Cu/Mn and Co/Mn systems and only diffraction rings are obtained (Figure 6b), although for all temperature regimes the materials maintain the same degree of chemical homogeneity. This is illustrated

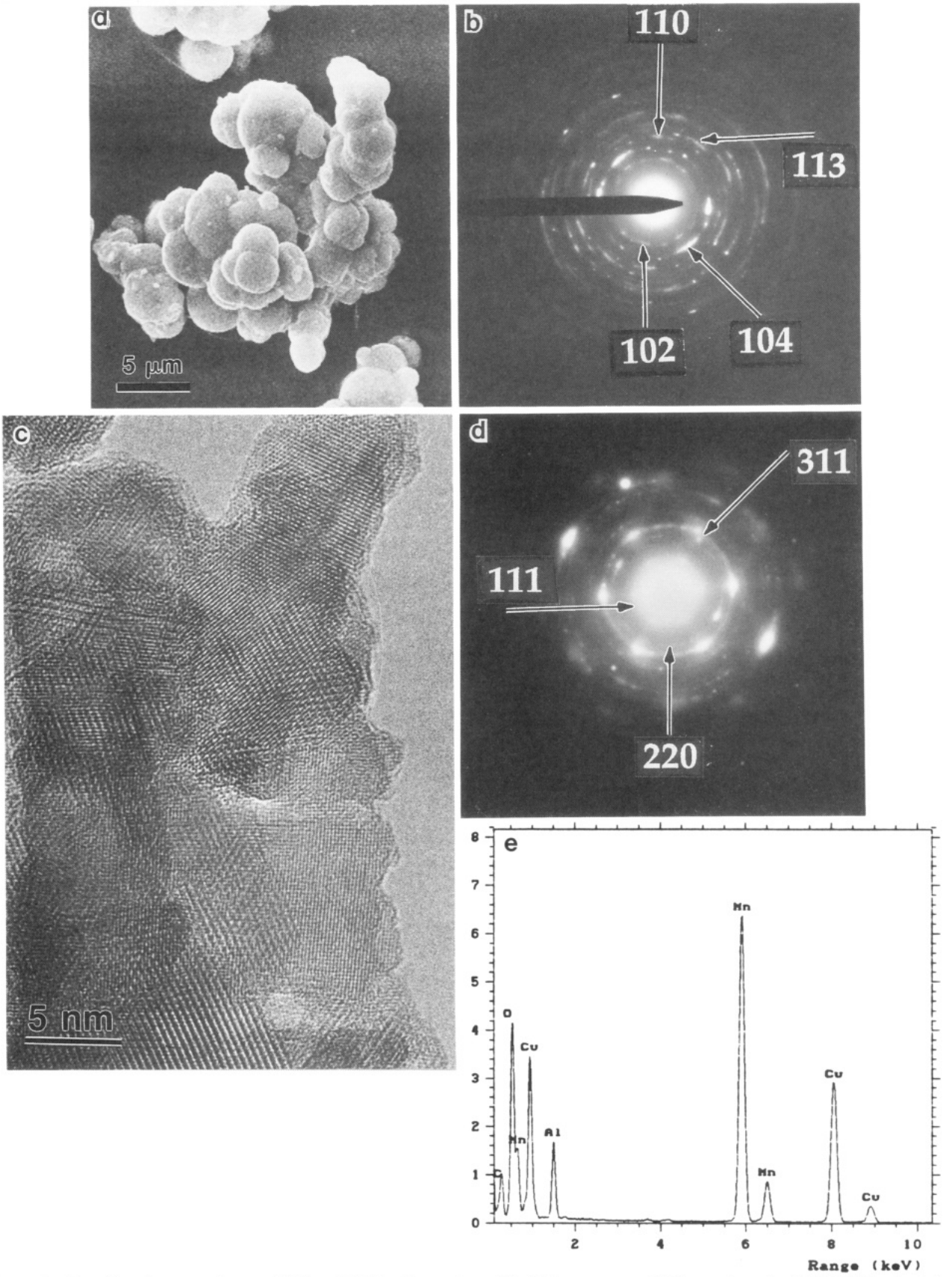

Figure 4. Scanning electron micrograph (a) and diffraction pattern (b) of the precursor $CuMn_2$ carbonate. HREM (c), selected area diffraction pattern (d), and electron-induced X-ray emission spectrum (e) of the corresponding spinel.

qualitatively by element maps of an agglomerate of spinel particles (Figure 6c–f). The quantification of the EDX data on five spot analyses gives a range of ca. 7% for each cation, showing that the cation stoichiometry is essentially ideal and indicating uniform substitution.

(d) Extended-Edge X-ray Absorption Spectroscopy (EXAFS). (*i*) *The Carbonates.* EXAFS of the Co and Mn K-edges of the cobalt manganese carbonate and of the Cu K-edge of the copper manganese carbonate were analyzed and Fourier transformed (without correction for

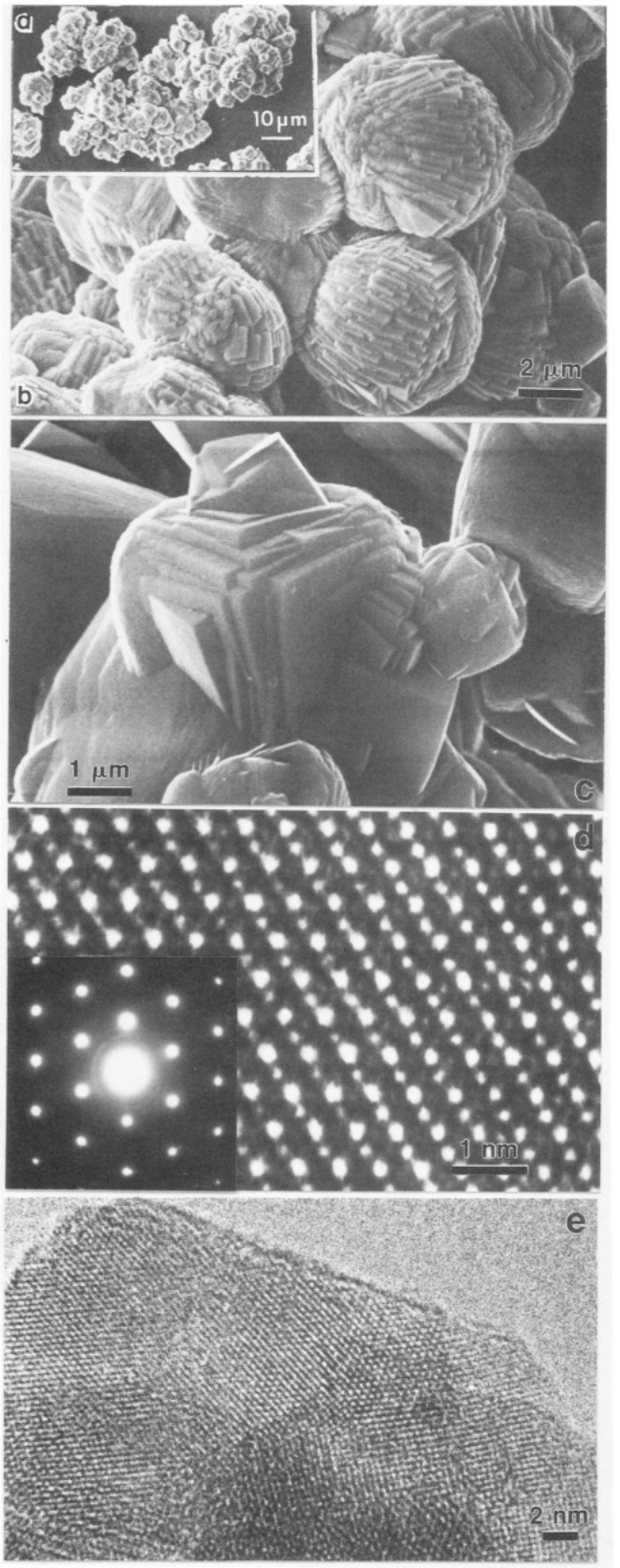

Figure 5. Scanning electron micrographs (a–c) and HREM and selected area diffraction pattern (d) of the $CoMn_2$ carbonate. HREM (e) of the corresponding spinel.

phase shifts). From these Fourier transforms, the peaks of which correspond to scattering shells, it is clear that the cobalt and manganese environments are nearly identical but are different from that of copper. This suggests that cobalt substitutes readily and with little distortion for manganese in the rhodocrosite structure whereas the copper environment is either highly distorted in the manganese site of rhodocrosite or is distributed between the rhodocrosite structure and an X-ray amorphous phase. First-shell fits to the EXAFS data indicate that the cobalt and manganese can be fitted as 6-fold coordinated to oxygens, with distances of 2.12 and 2.18 Å, respectively, while the first copper-oxygen shell is better fitted by four to give oxygens at 1.96 Å (the exact occupancy is sensitive to the window taken for Fourier filtering). Probably the remaining oxygens are Jahn–Teller distorted away from the copper.

Table II. Relevant Metal–Oxygen and Metal–Metal Distances below 4 Å for (a) Cubic and (b) Tetragonal Spinel Oxides

site	coord no.	atom type	dist, Å
	(a) $Cu_{1.5}Mn_{1.5}O_4$[16] ($Fd3m$)		
tetrahedral	4	O	1.967
	12	M[6]	3.437
	12	O	3.471
	4	M[4]	3.590
octahedral	6	O	1.978
	6	M[6]	2.931
	6	M[4]	3.437
	2	O	3.417
	6	O	3.651
	(b) $CoMn_2O_4$[17] ($I4_1/amd$)		
tetrahedral	4	O	2.015
	8	M[6]	3.427
	4	M[6]	3.703
	8	O	3.435
	4	O	3.787
	4	M[4]	3.678
octahedral	4	O	1.970
	2	O	2.140
	2	M[6]	2.890
	4	M[6]	3.057
	4	M[4]	3.427
	2	M[4]	3.703
	2	O	3.503
	2	O	3.689
	4	O	3.766

(ii) The Oxides. EXAFS analysis procedure: For the just-decomposed $CuMn_2$-420, CuMn-420, and CuCoMn-325 oxides the cations, and especially the copper, are in poorly ordered environments. In fitting the EXAFS, sufficient extra shells were added and refined to fit the data out to a distance (uncorrected for phase shifts) around 3.7 Å.

For the spinel structures, including the poorly crystalline just-decomposed $CoMn_2$ oxides, starting models for refinement were constructed using coordination numbers and bond distances of related spinel structures of the correct symmetry available in the chemical data base available at Daresbury ($CuMn_2O_4$, $Cu_{1.5}Mn_{1.5}O_4$, and Co_3O_4 (cubic) and $CoMn_2O_4$ (tetragonal)—see Table II) and assuming that the samples were stoichiometric. The spinel structure is usually written AB_2O_4, where A and B are cation sites of tetrahedral and octahedral coordination, respectively, within the cubic close-packed arrangement of oxygen ions. As with other spinels, mixed metal manganese-containing spinels offer the possibility of partition of different metals, often in more than one oxidation state, between the two sites, which in turn affects the structural, electrical and magnetic properties.[12–17]

(12) Buhl, R. *J. Phys. Chem. Solids* **1969**, *30*, 805.
(13) Boucher, B.; Buhl, R.; Perrin, M. *J. Appl. Phys.* **1968**, *39*, 632.
(14) Radhakrishnan, N. K.; Biswas, A. B. *Phys. Status Solidii A* **1977**, *44*, 45.
(15) Vandenberghe, R. E. *Phys. Status Solidii A* **1978**, *50*, K85.
(16) Vandenberghe, R. E.; Legrand, E.; Scheerlinck, D.; Brabers, V. A. M. *Acta Crystallogr.* **1976**, *B32*, 2796.

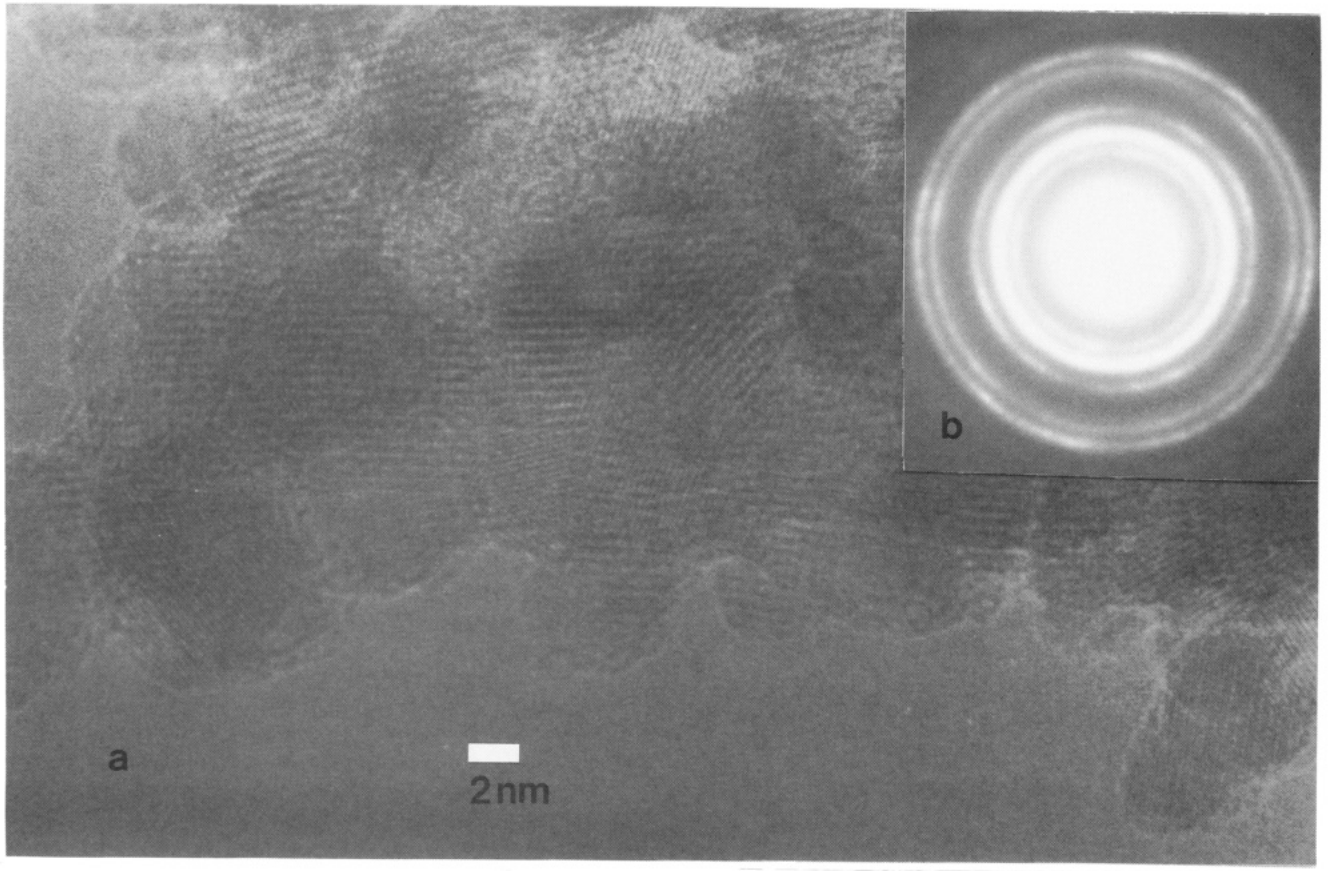

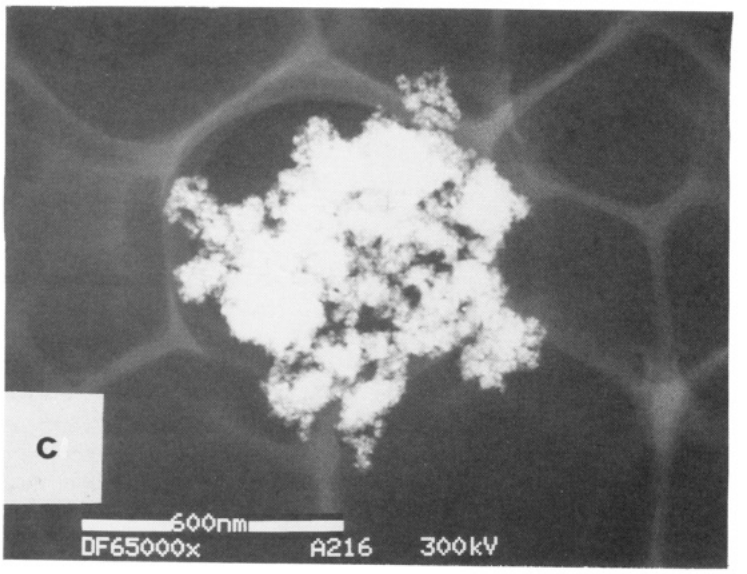

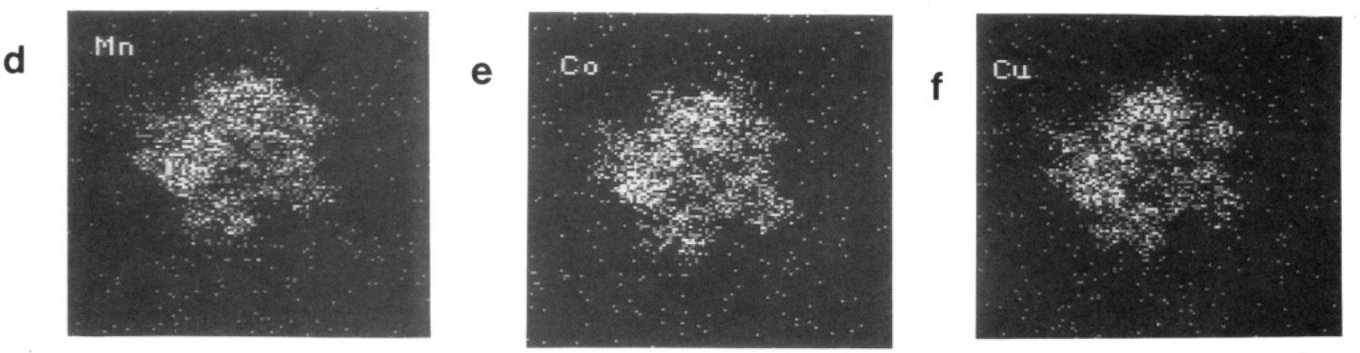

Figure 6. High-resolution micrograph (a) and selected area diffraction rings (b) of the $CuCoMnO_4$ spinel showing microcrystallites around 6 nm in dimension. SEM (c) and corresponding element maps (d–f) of the spinel particles, showing qualitatively that manganese, cobalt, and copper are homogenously distributed.

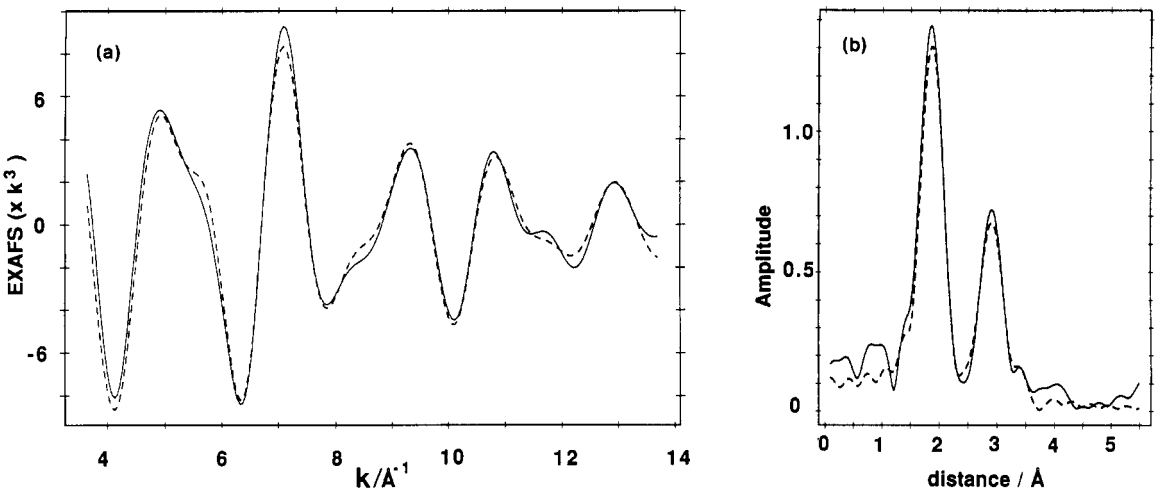

Figure 7. Experimental (solid line) and theoretical (dashed line) Fourier-filtered Mn K-edge EXAFS data (a) and their Fourier transforms (b) for the $CuMn_2$-420 amorphous oxide. The experimental Fourier transform is given unfiltered.

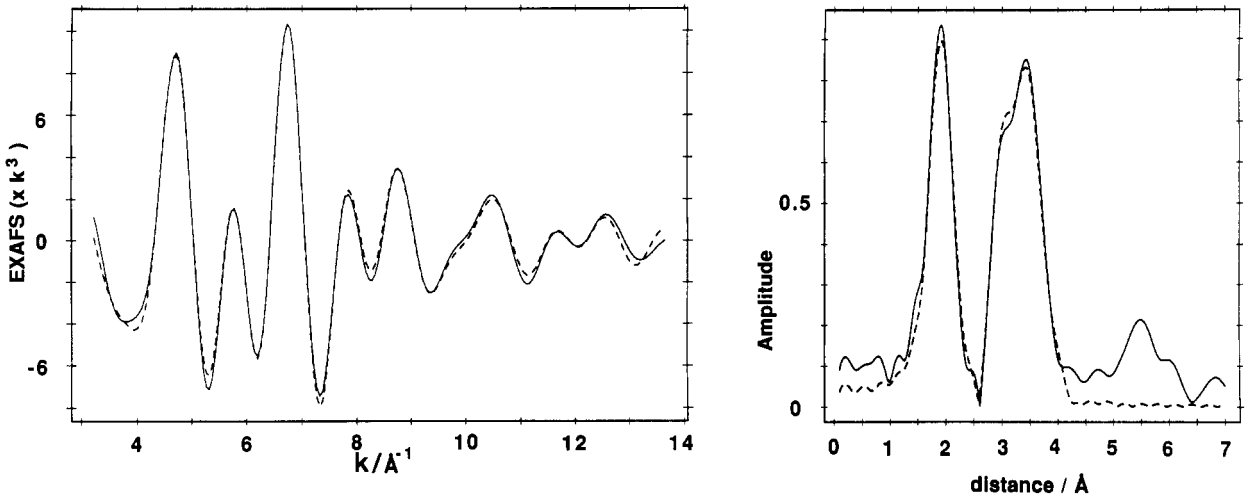

Figure 8. Experimental (solid line) and theoretical (dashed line) Fourier-filtered Cu K-edge EXAFS (a) and their Fourier transforms (b) for the $CuMn_2O_4$ spinel.

Initially, the first metal-to-oxygen coordination shell was Fourier filtered from the EXAFS data and fitted by allowing the M–O distance, the coordination number (N), and the Debye–Waller factor to refine. Deviation in the fitted coordination number from 4 (tetrahedral) or 6 (octahedral) was taken to indicate a distribution of the metal between the two sites, which varied for each metal in each sample. An estimate of x (the fraction of metal cations in tetrahedral coordination) was made using the simple relationship

$$N_{\text{average}} = xN_{\text{tetrahedral}} + (1 - x)N_{\text{octahedral}}$$

where $N_{\text{tetrahedral}}$ is 4, $N_{\text{octahedral}}$ 6. By mixing the octahedral and tetrahedral site occupancies and bond distances according to x, starting models were constructed to fit the EXAFS data out to around 3.7 Å. Since there were more shells than resolved peaks in the EXAFS function, the refinement was confined to distances and Debye–Waller factors. Once the higher shells had been fitted, the first coordination shell was also further refined again as a single shell (except for the manganese in the tetragonal, Jahn–Teller distorted $CoMn_2$-500 spinel; in this, the first shell was allowed to split into two). If the new refined value for $N1$ was outside experimental error of the first value of x, a new tetrahedral/octahedral distribution was constructed and refined (except for CuMn-500, where traces of CuO were observed in the XRD). The final value of x for each spinel is given in Table III but should be taken only as a rough estimate of the distribution, given the error associated with refined values of the coordination number.

The refined average coordination numbers, metal–oxygen distances, and Debye–Waller factors for the first coordination shells of amorphous and spinel oxides are given in Table III and representative fits to the EXAFS data are given in Figures 7–10. The analyses of the copper-bearing oxides and the cobalt-bearing oxides are described separately.

Copper-Bearing Amorphous Oxides: $CuMn_2$-420, CuMn-420, and CuCoMn-325. The Mn and Cu K-edge Fourier transforms of the amorphous $CuMn_2$-420 oxide are compared with those of the spinel $CuMn_2$-500 in Figure 11. The manganese ions have more order to the second shell than the copper. Similarly, and to a greater extent, the cobalt in CuCoMn-325 is more ordered than the copper in the same oxide.

Analysis of the first coordination shell of the copper in all the amorphous oxides gives a value close to 4 (Table III). There is no evidence for Jahn–Teller distorted oxygen at a greater distance. Analysis of the second peak in the Fourier transform indicates a copper–metal interaction at 2.88 Å for all samples, as well as other shells further away.

(17) Yamamoto, N.; Kawano, S.; Achiwa, N.; Higashi, S. *J. Jpn. Soc. Powder Metall.* **1983**, *30*, 48.

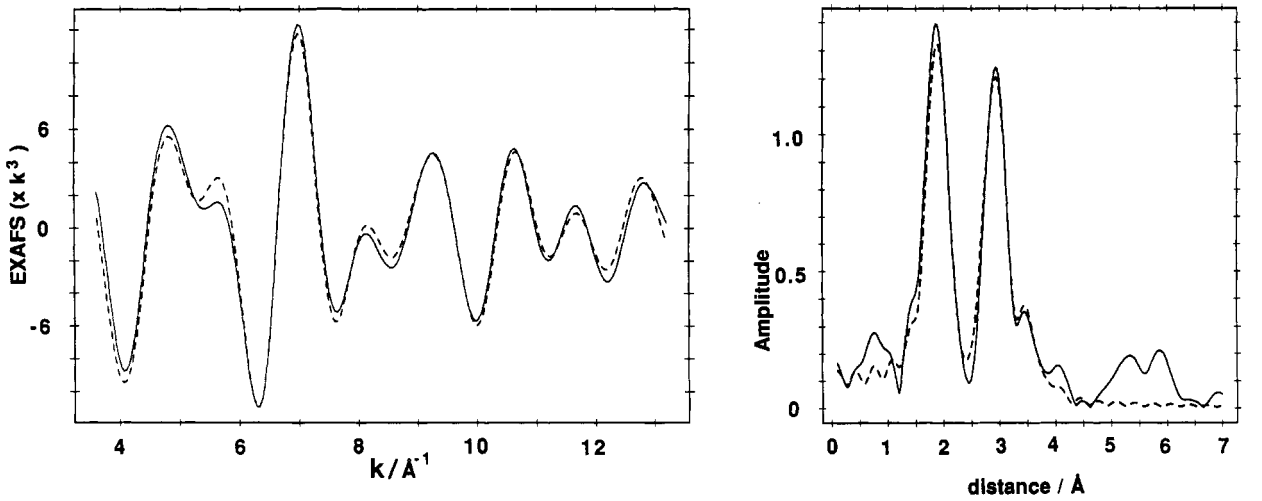

Figure 9. Experimental (solid line) and theoretical (dashed line) Fourier-filtered Mn K-edge EXAFS (a) and their Fourier transforms (b) for the $CuMn_2O_4$ spinel.

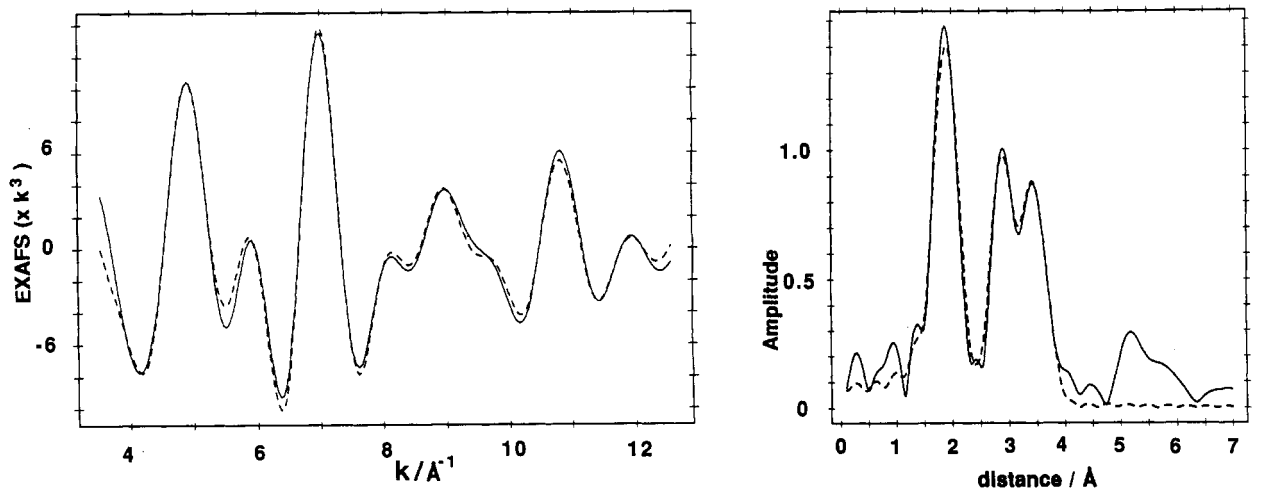

Figure 10. Experimental (solid line) and theoretical (dashed line) Fourier-filtered Co K-edge EXAFS (a) and Fourier transforms (b) for $CoMn_2O_4$ (415 °C).

Table III. First-Shell Metal–Oxygen Coordination Fits (One Shell Only unless Clearly Jahn–Teller Distorted)

		N_1	R_1	A_1	x
Cu K-edge	$CuMn_2$-420	4.1	1.935	0.014	
	$CuMn_2$-500	4.5	1.960	0.016	0.75
	CuCoMn-325	4.3	1.931	0.014	
	CuCoMn-500	4.2	1.937	0.014	0.80
	CuMn-420	4.5	1.928	0.015	
	$Cu_{1.5}Mn_{1.5}$-500	4.2	1.950	0.015	0.67
Co K-edge	CoCuMn-325	5.4	1.939	0.017	
	CoCuMn-500	6.0	1.939	0.010	0.1
	$CoMn_2$-415	5.5	1.943	0.013	0.33
	$CoMn_2$-430	5.2	1.948	0.013	
	$CoMn_2$-450	4.9	1.948	0.013	
	$CoMn_2$-500	4.6	1.961	0.011	0.75
Mn K-edge[a]	Mn_2Cu-420	5.3	1.907	0.010	
	Mn_2Cu-500	5.9	1.926	0.011	0.125
	Mn_2Co-430	5.3	1.902	0.010	
	Mn_2Co-500[b]				
	shell 1	4.0	1.910	0.007	0.25
	shell 2	1.3	2.237	0.016	
	MnCuCo-500	5.9	1.932	0.008	0.0

[a] MnO_2 used as model compound. Add 0.02 Å to bond lengths to calibrate on MnO model. [b] Two shells due to Jahn–Teller distortion. N_1, coordination number (accuracy 10%); R_1, coordination distance in Å (accuracy 0.02 Å; A_1, Debye–Waller factor Å^2; x, estimate of fraction of metal cations in tetrahedral sites (spinel).

This is the distance expected for octahedral copper in a spinel or square planar within CuO.

The EXAFS of Mn (in $CuMn_2$-420) and of Co (in CuCoMn-325) reveal coordination numbers around 5.4. The second shell in both cases is best fitted by a metal–metal distance at around 2.88 Å, the distance for octahedral sites in a spinel. Indeed, the Fourier transforms are similar to those observed for higher temperature spinel products. A representative fit to the EXAFS of the amorphous oxides is given for the Mn K-edge of $CuMn_2$-420 in Figure 7.

The manganese and cobalt probably form spinel nuclei in the amorphous copper-bearing oxides, with copper ordering more slowly into the structure.

Copper-Bearing Spinels: (CuMn$_2$-500, CuMn-500, and CuCoMn 500). The Cu K-edge Fourier transforms of these spinels (Figure 12) are dominated by a first shell at ca. 1.6 Å (uncorrected) and a second, doublet, with peaks at 2.65 and 3.1 Å (uncorrected for phase shifts). Fitting coordination shells determined by the spinel's crystallography (Table IIa) indicates that the 2.65-Å peak can only be due to copper occupying octahedral sites, the amount of which increases in the order CuCoMn < $CuMn_2$ < CuMn.

Fitting using EXCURV90 indicates that around one-quarter to one-third of the copper occupies octahedral sites in $CuMn_2$-500 and a slightly lower proportion in CuCoMn-500. For CuMn-500 the higher shells indicate more copper in octahedral coordination but the first-shell coordination number suggests that there is slightly less. This might be due to traces of copper oxide. An example of a fit, with a phase-corrected Fourier transform, is given in Figure 8

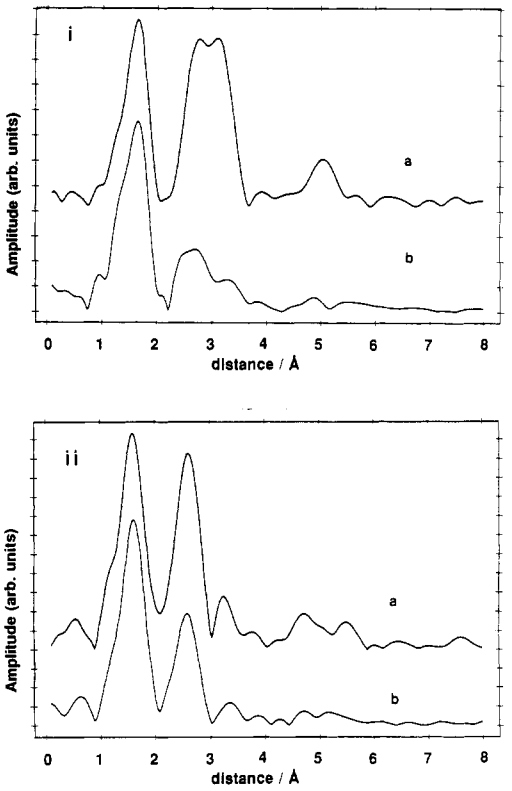

Figure 11. (i) Fourier transforms (phase shift uncorrected) of the Cu K-edge of the $CuMn_2$ (a) spinel and (b) amorphous oxides. (ii) Fourier transforms (phase shift uncorrected) of the Mn K-edge of the $CuMn_2$ (a) spinel and (b) amorphous oxides.

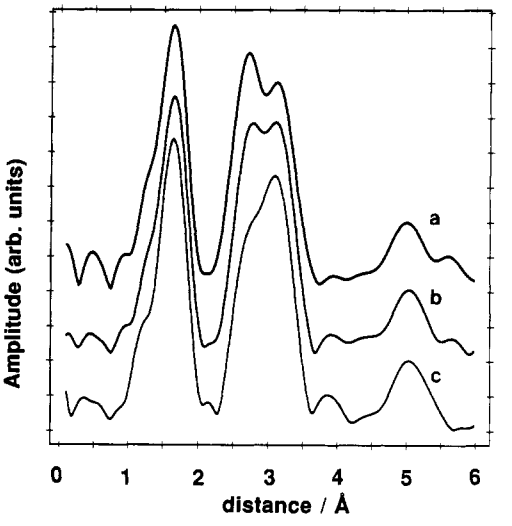

Figure 12. Fourier transforms of the Cu K-edge EXAFS (uncorrected for phase shifts) for (a) $Cu_{1.5}Mn_{1.5}O_4$, (b) $CuMn_2O_4$, and (c) $CuCoMnO_4$ spinels.

for $CuMn_2$-500, with three-quarters of the copper in tetrahedral sites.

The Mn K-edge Fourier transforms of the copper-bearing spinels $CuMn_2$-500 and CuCoMn-500 are rather similar, with two main peaks at ca. 1.7 and 2.7 Å (uncorrected) and a minor peak at 3.3 Å. The data are adequately fitted by manganese in a largely octahedral environment (for CuCoMn-500 the fitted coordination number is 6.0 and for $CuMn_2$-500 it is 5.9, both with bond lengths of 1.93 Å). The refined $CuMn_2$-500 Mn K-edge data are given as a representative fit (Figure 9).

Cobalt-Bearing Oxides. Fourier transforms of the cobalt K-edge EXAFS, given in Figure 13, show considerable variation, with peaks at 1.6, 2.6, and 3.15 Å (uncorrected)

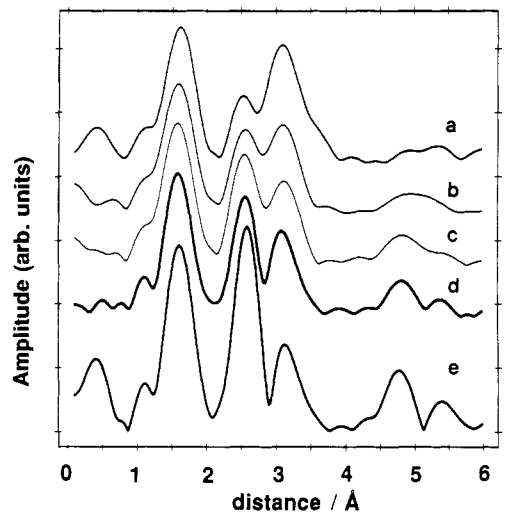

Figure 13. Fourier transforms (phase shift uncorrected) of the Co K-edge EXAFS for (a) $CoMn_2O_4$ (500 °C), (b) $CoMn_2O_4$ (450 °C), (c) $CoMn_2O_4$ (430 °C), (d) $CoMn_2O_4$ (415 °C), and (e) $CoCuMnO_4$.

that vary in intensity between samples. These differences are due to the cobalt occupying octahedral and tetrahedral sites in different ratios and in the symmetry change observed in the $CoMn_2$ spinel.

For the cubic CuCoMn spinel the cobalt K-edge is fitted very well by a well-ordered single-site octahedral environment, with M–O distances of 1.94 Å. In its amorphous precursor the cobalt has a slightly lower average coordination (5.4).

In the cubic $CoMn_2$-415 and $CoMn_2$-430 samples the cobalt exists in both tetrahedral and octahedral sites. Indeed, the first- and second-shell data are well fitted using Co_3O_4 as a starting model with a statistical distribution of cobalt in tetrahedral and octahedral sites (i.e., one-third tetrahedral and two-thirds octahedral; Figure 10). The manganese spectrum of $CoMn_2$-430 is close to that of CuCoMn-500, where manganese is predominantly octahedral. A simple model with statistical distribution of cobalt and manganese throughout the poorly crystalline cubic phase does not fit the EXAFS data. It may be that locally cobalt-rich spinels are formed, but the electron microscopy has not so far revealed this.

In the $CoMn_2$-500 Jahn–Teller distorted tetragonal spinel the average cobalt coordination decreases and the metal–oxygen distances increase. Although this is compatible with a migration of cobalt from octahedral to tetrahedral sites and subsequent reduction of Co from 3+ to 2+, it should be noted that cobalt in the octahedral sites might experience cooperative Jahn–Teller distortion which would complicate the analysis. No Jahn–Teller distorted long Co–O distances could be refined. A reasonable second-shell fit is obtained with cobalt distributed 3:1 between tetrahedral and octahedral sites. The model of cobalt migration is also backed up by the pre-edge (1s → 3d) features of the cobalt and manganese XANES, the cobalt preedge increasing slightly and the manganese pre-edge showing a slight decrease.

Although refinement of the Mn K-edge EXAFS of the $CoMn_2$-500 sample (which exhibits splitting of the second coordination shell peak at 2.7 Å (uncorrected) found in the Mn K-edge EXAFS of the cubic spinels into two peaks at 2.7 and 3.4 Å (uncorrected) as a result of Jahn–Teller distortion) is not sensitive to changes in the octahedral occupancy between about 65–85%, the data are well fitted by a model in which manganese exists 25% in tetrahedral and 75% in Jahn–Teller distorted octahedral coordination,

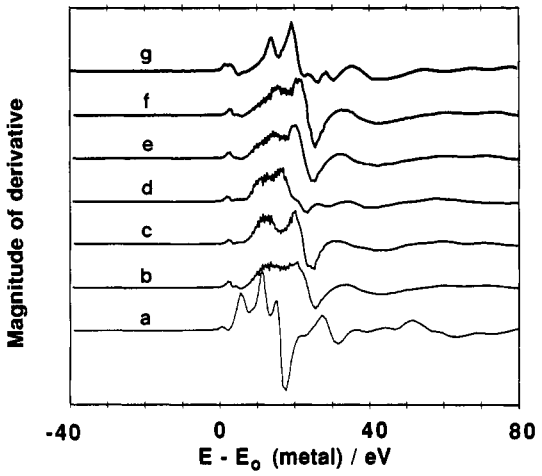

Figure 14. First derivative spectra of the region around the Mn K-edge of (a) MnO, (b) $CoMn_2$-430, (c) $CoMn_2$-500, (d) Mn_2O_3, (e) $CuMn_2$-500, (f) CuCoMn-500, and (g) MnO_2.

with a starting model for coordination distances and bond lengths taken from literature values for tetragonal $CoMn_2O_4$.

(e) X-ray Absorption Near-Edge Structure (XANES). The near-edge spectra of the oxides give information on the metals' oxidation state.[18,19] The best way to compare spectra is using their first derivatives. In general, a first derivative peak shift to higher energies results from oxidation of the cations, although Cu_2O is an exception.

For the Mn K-edge XANES (Figure 14) the first-derivative spectra, when compared with the model compounds MnO, Mn_2O_3, and MnO_2, indicate that the oxidation state of Mn in $CoMn_2$-430 and -500 is around 3+ and in $CuMn_2$ and CoCuMn is between 3+ and 4+. This is supported by electron yield Mn L_{III}-edge spectra on $CuMn_2$-420 and -500 that show a doublet at 647–649 eV indicative of Mn^{3+}/Mn^{4+} mixed valence, at least at the surface (G. Cressey, personal communication and ref 20).

The Co K-edge XANES first-derivative spectra are compared with those of CoO and Co_3O_4 in Figure 15. The spectra of $CoMn_2$-430 and $CoMn_2$-500 are rather similar, the latter showing a small (1 eV) shift to lower energies and an increase in the ratio of the lowest energy first-derivative peak over the second peak, possibly due to 3+ → 2+ reduction of cobalt. The derivative spectrum of CuCoMn-500 has the same general features as $CoMn_2$-430 and Co_3O_4, but the order of size of the three derivative peaks suggests an average oxidation state greater than in the Co_3O_4 spinel and therefore probably around 3+. The copper first-derivative spectra are rather similar to each other but do suggest that $CuMn_2$-500 has a higher proportion of copper in 1+ than the other spinels. No compounds with tetrahedral Cu^+ or tetrahedral Cu^{2+} were available for comparison.

We are able to infer details on the siting and oxidation state of cations in the oxides by using information on coordination number, M–O distance, XANES derivative spectra, and, where applicable, the charge constraints imposed by the spinel structure, and also bearing in mind M–O distances predicted for different oxidation states from tables compiled from empirical data.[21]

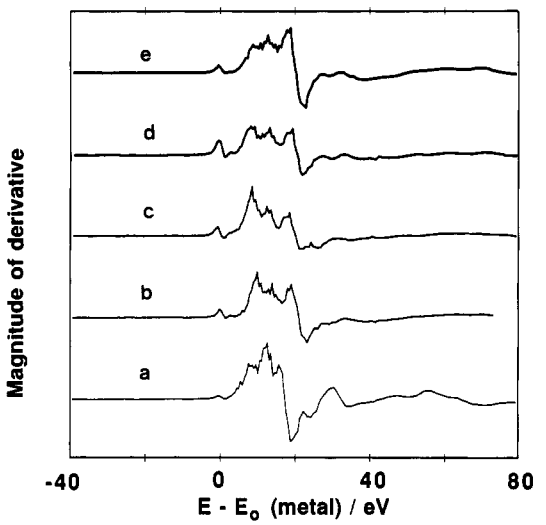

Figure 15. First derivative spectra of the region around the Co K-edge of (a) CoO, (b) $CoMn_2$-415, (c) $CoMn_2$-500, (d) Co_3O_4, and (e) CuCoMn-500.

For CuCoMn, which shows the least mixing of cations over different sites, cobalt is octahedral, with a Co–O distance of 1.94 Å corresponding to an oxidation state of 3+. Manganese also occupies octahedral sites, with a Mn–O distance of 1.93 Å. The XANES suggests an oxidation state between 3+ and 4+, and this agrees with bond length comparisons with the literature (Mn^{3+}[6]–O, 1.96 Å; Mn^{4+}[6]–O, 1.91 Å). As the oxidation state of manganese is between 3+ and 4+, the copper must have an average oxidation state between 1+ and 2+. The Cu–O distance of 1.94 Å is consistent with a mixture of Cu^{2+} and Cu^{1+} occupying the tetrahedral site. An estimate of the distribution would then be

$$Cu[4]2+,1+,\ Co[6]3+,\ Mn[6]4+,3+$$

A similar treatment can be performed for $CuMn_2$ and $CoMn_2$ spinels on which complete XANES data are available. The manganese oxidation state in $CuMn_2$ is a mixture of 3+ and 4+, indicating that copper must be present as 1+ and possibly 2+. In the $CoMn_2$-500 spinel, manganese is mainly 3+, i.e., d^4, and therefore tends to Jahn–Teller distort. Cobalt is therefore 2+ and 3+.

In summary, the EXAFS and XANES data give considerable information on the state of the cations in both the amorphous and spinel phases, despite the ambiguities caused by mixed site occupancies and oxidation states and the symmetry change induced by cooperative Jahn–Teller distortion in the cobalt manganese system. For the spinels studied, copper has the greatest tendency to go into tetrahedral sites, probably as 1+ and 2+ cations. The percentage tetrahedral occupancy of copper increases in the order

$$Cu_{1.5}Mn_{1.5} < CuMn_2 < CuCoMn$$

Cobalt in the poorly crystalline $CoMn_2$-430 is nearly statistically distributed between octahedral and tetrahedral sites but shows slight ordering on being heated to 500 °C. High enough concentrations of Mn^{3+} in the octahedral site cooperatively distort the structure.

Manganese is present mainly as 3+ in $CoMn_2$ and as 3+ and 4+ in $CuMn_2$ and CoCuMn-500. As a converse to cobalt and copper, manganese is always predominantly octahedral.

(f) Catalysis and Adsorption. Catalyst surface areas are given in Table IV. The CuCoMn oxides have particularly high surface areas. Catalytic conversion rates of CO,

(18) Brown, N. M. D.; McMonagle, J. B.; Greaves, G. N. *J. Chem. Soc., Faraday Trans 1* **1984**, *80*, 589.

(19) Belli, M.; Bianconi, A.; Mobilio, S.; Palladino, L.; Reale, A.; Burattini, E. *Solid State Commun.* **1988**, *35*, 355.

(20) Cramer, S. P.; de Groot, F. M. F.; Ma, Y.; Chen, C. T.; Sette, F.; Kipke, C. A.; Eichhorn, D. M.; Chan, M. K.; Armstrong, W. H.; Libby, E.; Christou, G.; Brooker, S.; McKee, V.; Mullins, O. C.; Fuggle, J. C. *J. Am. Chem. Soc.* **1991**, *113*, 7937.

(21) Shannon, R. D. *Acta Crystallogr.* **1986**, *A32*, 751.

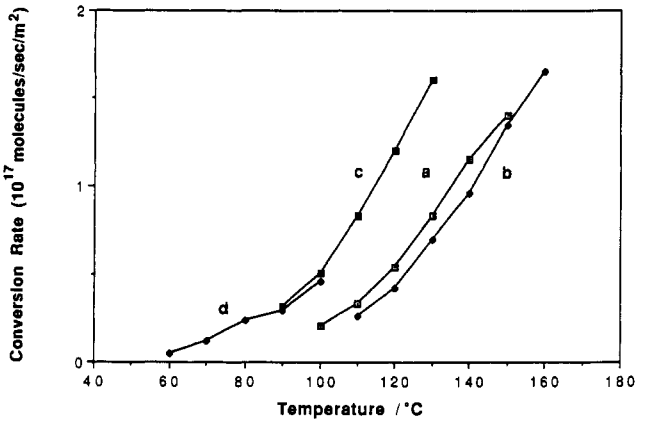

Figure 16. Conversion rates of CO to CO_2, normalized to catalyst surface area, as a function of temperature when a 1% CO (32% He) and air mixture was passed at 60 mL/min over 0.02 g of the amorphous, just-decomposed oxides mixed with 0.08 g of quartz: (a) $CuMn_2$, (b) $CoMn_2$, (c) CuMn, and (d) CuCoMn stoichiometries.

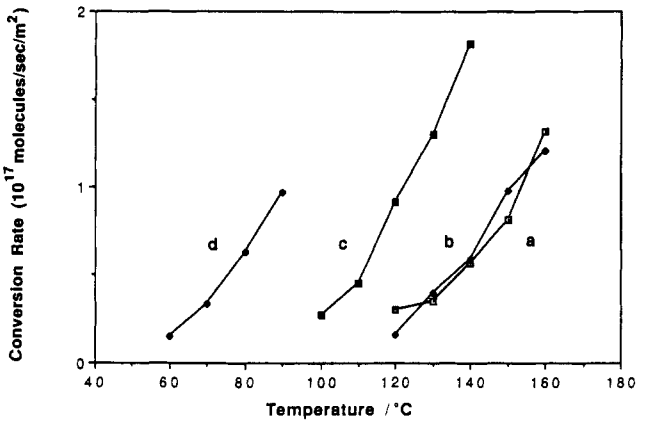

Figure 17. Conversion rates, measured and calculated as in Figure 16, for the spinel oxides (a) $CuMn_2O_4$, (b) $CoMn_2O_4$, (c) $Cu_{1.5}Mn_{1.5}O_4$, and (d) $CuCoMnO_4$.

normalized to surface area, are shown in Figures 16 and 17 for amorphous and spinel oxides respectively, and in Figure 18 for the single-metal oxides. The data are plotted only for temperatures where the total conversion was less than 100%. Direct comparison of specific activities of oxides at the same temperature is slightly complicated by the variation of the reactant concentration profile across the bed with the total conversion, but this has no effect on the general conclusions that may be drawn.

Discussion

The combination of X-ray diffraction, electron microscopy, and nanometer-scale microanalysis and X-ray absorption at the copper, cobalt, and manganese K-edges yields detailed information pertaining to the metal cation distribution in the coprecipitated carbonates, the spinels and the intermediate poorly crystalline or amorphous oxides.

The mixed metal carbonates contain only one crystalline phase and are, in general, homogeneous. If present, additional amorphous content must be low. The EXAFS of cobalt and manganese in $CoMn_2(CO)_3)_3$ are essentially identical, indicating complete substitution. Copper in $CuMn_2(CO_3)_3$ appears to be distorted, possibly as a result of expected Jahn–Teller effects in the rhodocrosite structure. All of the mixed metal carbonates show lattice parameters smaller than rhodocrosite as a result of incorporation of the smaller cobalt and copper, and the crystallinity decreases as more and smaller cations are incorporated into the structure.

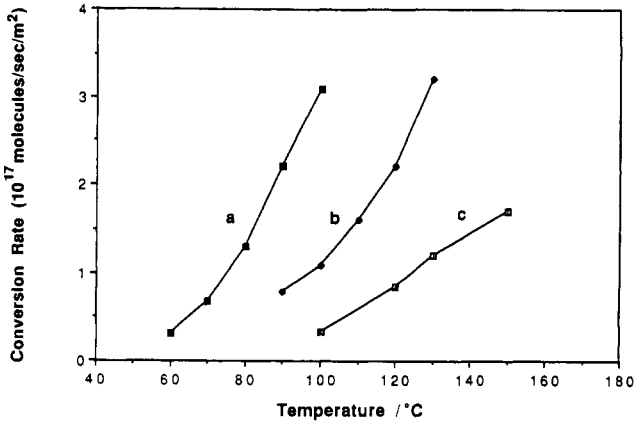

Figure 18. Conversion rates, measured and calculated as in Figure 16, for the metal oxides (a) Co_3O_4, (b) CuO, and (c) MnO_x.

Table IV. Surface Areas from BET Analysis of N_2 Adsorption Data at 77 K

sample	surface area, m^2/g	sample	surface area, m^2/g
$CuMn_2$-420	79	CuCoMn-325	188
$CuMn_2$-500	35	CuCoMn-500	113
CuMn-420	63	CuO	25
CuMn-500	39	MnO_x	33
$CoMn_2$-420	65	Co_3O_4	30
$CoMn_2$-500	39		

The amorphous oxides formed upon decomposing the copper-containing carbonates possess copper in 4-fold coordination (without additional Jahn–Teller distorted oxygens), but the data are insufficient to distinguish between square planar and tetrahedral variants. The bond lengths are around 1.93 Å, which favors a model with predominantly divalent copper.

The spinels formed in the copper-bearing systems are also monophasic to X-ray diffraction, with the exception of $Cu_{1.5}Mn_{1.5}$, which contains traces of CuO. All are cubic, and copper resides mainly in the tetrahedral site, with varying proportions in the octahedral site shown clearly by EXAFS. The copper–oxygen distances in the spinels (1.94–1.96 Å) are larger than in the amorphous oxides (ca. 1.93 Å). The oxidation state is a mixture of 1+ and 2+, on the basis of the XANES and EXAFS of the co-metals but quantification of the oxidation state is insufficiently precise to distinguish between models proposed for $CuMn_2O_4$ prepared by solid-state methods discussed in the literature.[14-16] The observation of a mixture of oxidation states is in agreement with XPS measurements on the surface of predominantly spinel oxides of the metal stoichiometries CuMn and CuCoMn.[5]

Cobalt in the mixed CuCoMn spinel occupies octahedral sites as 3+, low spin. In $CoMn_2$ spinels the EXAFS analysis is complicated by the transition from cubic to tetragonal on heating. The cubic form is a metastable result of the low-temperature route and is not observed in high-temperature solid-state preparations. The predominantly octahedral coordination of manganese in the low-temperature sample suggests either a defective spinel or local inhomogeneity. The cobalt appears to be statistically distributed in the cubic form and shows a small degree of ordering in the tetragonal form. This is to be expected from the site preference measured in samples quenched from high temperatures, where it is seen that while cobalt does show a preference for the tetrahedral sites, the degree of inversion varies strongly with temperature.[13]

Catalytic performance can be rationalized with reference to the bulk structural features, recognizing likely differ-

ences in surface and bulk composition. Amorphous and spinel phase oxides in the Cu/Mn and Co/Mn systems have similar specific activities (i.e., activity per unit surface area), the slightly lower specific activity of the spinels possibly being due to a reduction of the oxidation state of the copper and cobalt suggested by EXAFS and XANES. For the CuCoMn oxides, the lower specific activity of the amorphous compared with the spinel oxide may be due to incomplete carbonate decomposition at the low temperature (325 °C) employed. Among the spinels, the CuCoMn spinel possesses much higher specific activity than the others. Direct comparison with the $CuMn_2$-spinel, where copper is also in both 1+ and 2+ oxidation states and manganese 3+ and 4+, suggests that the presence of Co^{3+} is responsible for the high activity. This is supported by the high specific activity of the spinel Co_3O_4, where two-thirds of the cobalt is trivalent, and the comparatively low activity of $CoMn_2O_4$, which contains a high proportion of cobalt as 2+ (tetrahedral). The specific activity of Co_3O_4 is around twice that of $CuCoMnO_4$ and can be explained by Co_3O_4 having, per unit cell, twice as much Co^{3+} as $CuCoMnO_4$. The 3-fold higher surface area of $CuCoMnO_4$ than Co_3O_4 makes it the most active of the catalysts examined. Manganese 3+/4+ is relatively inactive in the $CoMn_2$, $CuMn_2$, and MnO_x oxides. The higher activity of the $Cu_{1.5}Mn_{1.5}O_4$ spinel compared to $CuMn_2O_4$ might be due to a higher proportion of copper being divalent (CuO is more active than the MnO_x oxide).

Of the various mixed metal oxide catalysts examined here for the low-temperature oxidation of CO to CO_2, the best is undoubtedly the $CuCoMnO_4$ spinel: its intrinsic activity is high; it also has good thermal stability and may be readily prepared in a high area form.

Acknowledgment. We acknowledge the SERC for its support, in particular the guidance of Professor G. N. Greaves at the Daresbury Synchrotron Laboratory. We also thank Du Pont management for encouraging collaboration between the Central Experimental Station and the Royal Institution. We are grateful for the SERC chemical database service, and we thank Dr. G. Sankar and Professor C. R. A. Catlow for stimulating discussions.

Hydrothermal Syntheses and Structural Refinements of Single Crystal $LiBGeO_4$ and $LiBSiO_4$

J. B. Parise*

CHiPR† and Department of Earth and Space Sciences, State University of New York, Stony Brook, New York 11794

T. E. Gier

Central Research and Development Department, E. I. DuPont de Nemours & Co., Inc., Experimental Station, Wilmington, Delaware 19880

Received April 6, 1992. Revised Manuscript Received June 27, 1992

The low-temperature form of $LiBGeO_4$ and the new composition $LiBSiO_4$ have been synthesized as single crystals for the first time by employing a hydrothermal recrystallization technique. They have been studied using single-crystal X-ray diffraction. These compounds possess the cristobalite structure, crystallizing in the tetragonal space group $I\bar{4}$ with $Z = 2$. The absence of a center of symmetry was confirmed by a second harmonic generation test. The cell parameters are $a = 4.5016$ (3), $c = 6.901$ (3) Å for $LiBGeO_4$ and $a = 4.3792$ (2), $c = 6.7784$ (3) Å for $LiBSiO_4$. The lithium atoms are well ordered into sites with approximately tetrahedral geometry.

Introduction

The family of stuffed, ordered cristobalite structures ($MABO_4$) crystallize in the noncentrocymmetric space group $I\bar{4}$ and have therefore been considered as possible materials for nonlinear optical applications.[1] Lithium borogermanate, $LiBGeO_4$, is believed to belong to this class of materials. It melts congruently at about 900 °C, and crystals have been grown by sufficiently slow cooling of the extremely viscous melt. However, differences of opinion persist concerning details of the structure of this material.[1-3] Specifically, Ihara[2] claims the structure is orthorhombic, pseudotetragonal, while more recent publications[2,3] propose a tetragonal cell, space group $I\bar{4}$. Unfortunately, only twinned crystals have been obtained from slow cooling of the melt, and these are unsuitable for single-crystal diffraction measurements.

In the course of a general survey of the structure–property relationships of members of the cristobalite family, we have grown crystals of $LiBGeO_4$ and $LiBSiO_4$ by hydrothermal techniques. The crystals of $LiBGeO_4$ were free of the twinning reported previously[2] and thereby provided an opportunity to accurately determine the crystal structure of this material. Further, for any potential optical applications untwinned single crystals are desirable; the hydrothermal technique provides a means of obtaining such materials.

The composition $LiBSiO_4$ is novel, and this material is expected to be isostructural with $LiBGeO_4$; the synthesis and structure of $LiBSiO_4$ are reported for the first time.

Experimental Section

Synthesis and Characterization. Small single crystals of $LiBGeO_4$ were grown hydrothermally in a sealed gold capsule containing appropriate quantities of preformed $LiBGeO_4$ powder (12 wt %) and 2 M H_3BO_3 (88 wt %). After the capsule was

† The Center for High Pressure Research: An NSF funded Science and Technology Center.

(1) Rulmont, A.; Tarte, P.; Winand, J. *J. Mater. Sci. Lett.* **1987**, *6*, 659.
(2) Ihara, M. *Jpn. J. Ceram. Assoc.* **1971**, *79*, 152.
(3) Liebertz, J.; Stähr, S. *Z. Kristallogr.* **1981**, *155*, 115.

0897-4756/92/2804-1065$03.00/0